IET Generation, Transmission & Distribution

Research Article

IET Journals
The Institution of Engineering and Technology

Distributed control scheme on cost optimisation under communication delays for DC microgrids

ISSN 1751-8687
Received on 1st November 2016
Revised 1st June 2017
Accepted on 12th July 2017
E-First on 25th August 2017
doi: 10.1049/iet-gtd.2016.1716
www.ietdl.org

Hua Han[1], Hao Wang[1], Yao Sun[1] ✉, Jian Yang[1], Zhangjie Liu[1]

[1]*Department of Information Science and Engineering, Central South University, Minzhu Building, Changsha, People's Republic of China*

✉ *E-mail: yaosuncsu@gmail.com*

Abstract: This study addresses the distributed economic dispatch problem for DC microgrids when time-varying delays are present in communication networks. A novel distributed algorithm is proposed, and the proposed controller contains a distributed generation cost optimisation module and a voltage regulation module. The cost optimisation module is aimed to realise cost optimisation by driving the incremental cost rate of every distributed generator to be equal. In the voltage regulation module, a distributed synchronisation algorithm is used to restore the global average voltage. After the effect of the communication delay on the system stability is analysed, the robust stability criticality under load changes is obtained by using linear matrix inequality. The performance of the proposed scheme is validated through simulations and experimentally.

1 Introduction

A resurgence in the use of DC microgrids is occurring because of the development and deployment of distributed generators (DGs), such as solar photovoltaic, wind power electric, and energy storage generators, which offer inherent advantages for loads in commercial, industrial, and residential applications [1]. As compared with AC microgrids, DC microgrids have unique advantages, such as high capacity transmission lines, a highly reliable power supply, and less system loss. Furthermore, the transformer inrush current, frequency synchronisation, and reactive power flow do not need to be considered [2, 3].

Many studies have been conducted in recent years on economic optimisation in DC microgrids. The centralised control strategy, with its benefits in terms of maximising economic operation and satisfying voltage regulation, is widely applied in DC microgrids [4, 5]. However, the need for strong communication systems and the complicated centralised controller increase the operating cost, control complexity, and communication infrastructure, which may result in poor power control and low reliability.

Decentralised control has been developed to replace centralised control, owing to its excellent characteristics, such as high-level reliability and simple communication network requirements [6–8]. As a classical decentralised control method, conventional droop control achieves power sharing among DGs in microgrids [9]. However, proportional power sharing based on power ratings alone can ensure only that the generated power is proportional to the capacity of a DG, which may not achieve economical operation. A cost-based droop scheme in which droop control and economic optimisation were combined was proposed for obtaining lower generation costs for microgrids [10, 11]. These approaches reduce the operating costs of a microgrid to a certain extent, which represents a major milestone in microgrid operation optimisation. However, droop mechanisms sometimes suffer from poor voltage regulation and load sharing, particularly when the distribution line impedances cannot be negligible [12, 13].

Since they combine the merits of both centralised and decentralised approaches, the use of distributed methods in DC microgrids has become increasingly widespread [14–21]. The dynamic consensus algorithm is a crucial technique in the distributed methods for economic optimisation and can be designed to achieve power sharing [14–18], voltage restoration [19, 20], and current sharing [21]. To achieve cost optimisation, an incremental cost rate λ-consensus method was proposed to realise economic optimisation [14, 15]. In [16], a gradient-based distributed method was also applied to solve the cost optimisation problem in DC microgrids. However, the step size should be carefully chosen when the variables reach their constraint bounds. In order to improve power quality, distributed consensus control methods were proposed for realising optimal power allocation and voltage recovery [17, 18]. Time delay arising from communication is not a negligible factor in consensus control design. However, none of these methods considers a theoretic analysis of the communication delay.

The main problem involved in consensus with time delay is the effects of time delay on the convergence and performance of consensus [22–26]. Using linear matrix inequality (LMI), a consensus algorithm for directed networks with time-varying delays was investigated in [24]. Recently, optimisation in distributed multi-agent coordination has been studied in terms of convergence speed [25] and certain specific cost functions [26]. In DC microgrids based on distributed optimisation control, a communication delay even has a destabilising effect on the system. Thus, considering a constant communication delay, in [27, 28] the stability of the distributed optimisation DC microgrid was analysed with a discrete-time model. The effect of communication delays on the convergence of an economic dispatch algorithm was analysed, and the maximum allowable communication delay bounds were derived by the generalised Nyquist criterion. In [18], the effects of time delays on the economic dispatch algorithm were examined only through simulations. Thus far, no report on the distributed cost optimisation of DC microgrids under load variations when time-varying delays are present has been published.

For DC microgrids with a time-variable delay in the communication network, this paper proposes a distributed optimisation control method to minimise the total cost of power generation and restore the global average voltage. Regarding cost optimisation, each DG exchanges only the estimated value of the incremental cost rate with neighbours, which reduces the dependence on the communication bandwidth; the output power of each DG is based on the equal incremental principle to achieve cost optimisation. In addition, in this study, we explored the influence of time-varying delays and analysed the robust stability criticality of the system, taking communication delays and load parameter uncertainties into consideration. The contributions of this paper are summarised as follows:

(i) A distributed cost optimisation control method that takes time-varying communication delay into consideration is proposed.

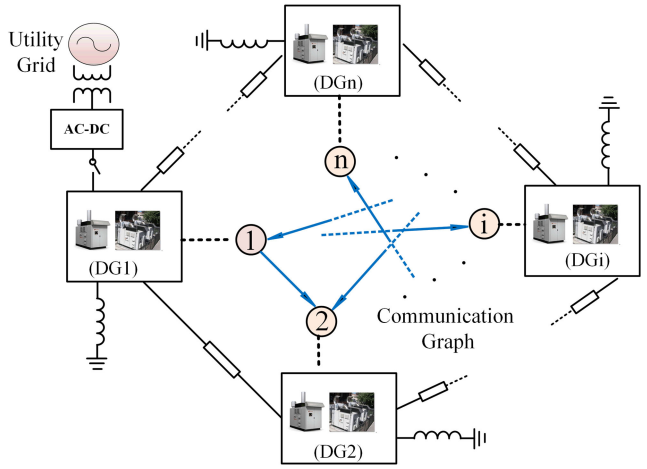

Fig. 1 *Configuration of communication and physical connection*

(ii) It is shown that, when the load varies under communication delay conditions, the control method can also be used, and a satisfactory transient process can be achieved.
(iii) The criticalities of the robust stability of the system are obtained by LMI.

2 Cost optimisation problem of DC microgrids

2.1 Cost functions for DC distributed generators

In general, the generation cost of a DG depends on its operational characteristics and rating. Therefore, the generation costs of different DGs cannot be represented by a common function. The distributed system examined in this study is shown in Fig. 1.

The common cost functions of conventional generators, such as diesel generators, micro turbines, and energy storage equipment, are represented as [12]

$$C_i(P_i) = K_{m,i}P_i + K_{f,i}\left(a_i + b_iP_i + c_iP_i^2\right) + K_{\xi,i}\left(\alpha_i + \beta_iP_i + \gamma_iP_i^2 + \varepsilon_i\exp(\rho_iP_i)\right) \tag{1}$$

where i represents the DG number, P_i is the output power of the ith DG, constants a_i, b_i, and c_i represent the fuel consumption behaviour of the combustion engine, α_i, β_i, γ_i, ε_i, and ρ_i represent the emission penalty or incentive, and $K_{m,i}$, $K_{f,i}$, and $K_{\zeta,i}$ are the equivalent cost coefficients of the active power, consumption of the combustion engine, and emission penalty, respectively.

Being of different types, the cost functions of dispatchable green sources, such as fuel cell, wind, and photovoltaic sources, with storage components can be alternatively derived from their direct operating costs and converter loss-efficiency functions [13, 29]

$$C_i(P_i) = K_{o,i}\left(P_i + K_{l,i}\left(v_i + u_iP_i + w_iP_i^2\right)\right) \tag{2}$$

where $K_{O,i}$, $K_{l,i}$, v_i, u_i, and ω_i are constants for the considered source.

In fact, in addition to the DGs mentioned above, in DC microgrids, energy storage systems (ESSs) are important components. However, the generation cost function for the energy storage can be approximately seem as that of conventional power generation units [18]. Thus, this paper does not specifically discuss the cost of ESS, and presents several common DGs as an example to explore the effectiveness of the proposed control.

To compare the cost of all DGs on an equal scale, all the cost functions were normalised based on their respective power ratings, as given by

$$P_i' = \frac{P_i}{P_{\max,i}}, \quad C_i'(P_i) = C_i(P'_i) \tag{3}$$

where $C_i'(P_i)$ $(i = 1, 2, \ldots, n)$ represents the DGs' cost functions.

2.2 DC microgrid cost optimisation problem

Mathematically, the minimum generation cost can be obtained by solving the following optimisation problem. The objective function is represented as

$$J = \min \sum_{i=1}^{n} C'_i(P_i) \tag{4}$$

First, the output power of all the DGs in a DC microgrid must meet the requirement of the total loads

$$P_{\text{load}} = \sum_{i=1}^{n} P_i \tag{5}$$

According to the given objective function and constraints, the Lagrange function is established as

$$L(P_1, P_2, \ldots, P_n, \lambda) = \sum_{i=1}^{n} C'_i(P_i) - \lambda\left(\sum_{i=1}^{n} P_i - P_{\text{load}}\right) \tag{6}$$

where λ is the Lagrange multiplier. Thus, the conditional extremum problem is changed into a non-constrained optimal problem. Because the cost function is strictly convex and differentiable, the minimum of the Lagrange function is achieved by solving the equations

$$\begin{cases} \dfrac{\partial L}{\partial P_i} = \dfrac{\partial C'_i(P_i)}{\partial P_i} - \lambda = 0 \\ \dfrac{\partial L}{\partial \lambda} = \displaystyle\sum_{i=1}^{n} P_i - P_{\text{load}} = 0 \end{cases} \quad (i = 1, 2, \ldots, n) \tag{7}$$

Then, we obtain

$$\begin{aligned} &\frac{\partial C'_1(P_1)}{\partial P_1} - \lambda = \frac{\partial C'_2(P_2)}{\partial P_2} - \lambda = \cdots \\ &= \frac{\partial C'_n(P_n)}{\partial P_n} - \lambda = \sum_{i=1}^{n} P_i - P_{\text{load}} = 0 \end{aligned} \tag{8}$$

Let $f_i(P_i) = ((\partial C'_i(P_i))/\partial P_i)$; then, we have

$$f_1(P_1) = f_2(P_2) = \cdots = f_n(P_n) = \lambda \tag{9}$$

Using (8) and (9), it is easy to obtain the optimal output voltage of each DG for centralised control, because centralised control can collect the cost increment rate, $\lambda_i(i = 1, 2, \ldots, n)$, of all the DGs. Then, each DG can generate power according to the optimal power distributed. However, the need for strong communication links and a complicated centralised controller increases the operating cost and control complexity, and thus, many studies were focused on the study of distributed control.

3 Distributed control methods with consideration of communication delay

In order to achieve both cost optimisation and voltage restoration when time-varying communication delays are present, a unified distributed control method is proposed.

3.1 Proposed distributed minimum-cost control scheme

A novel distributed synchronisation control method is proposed:

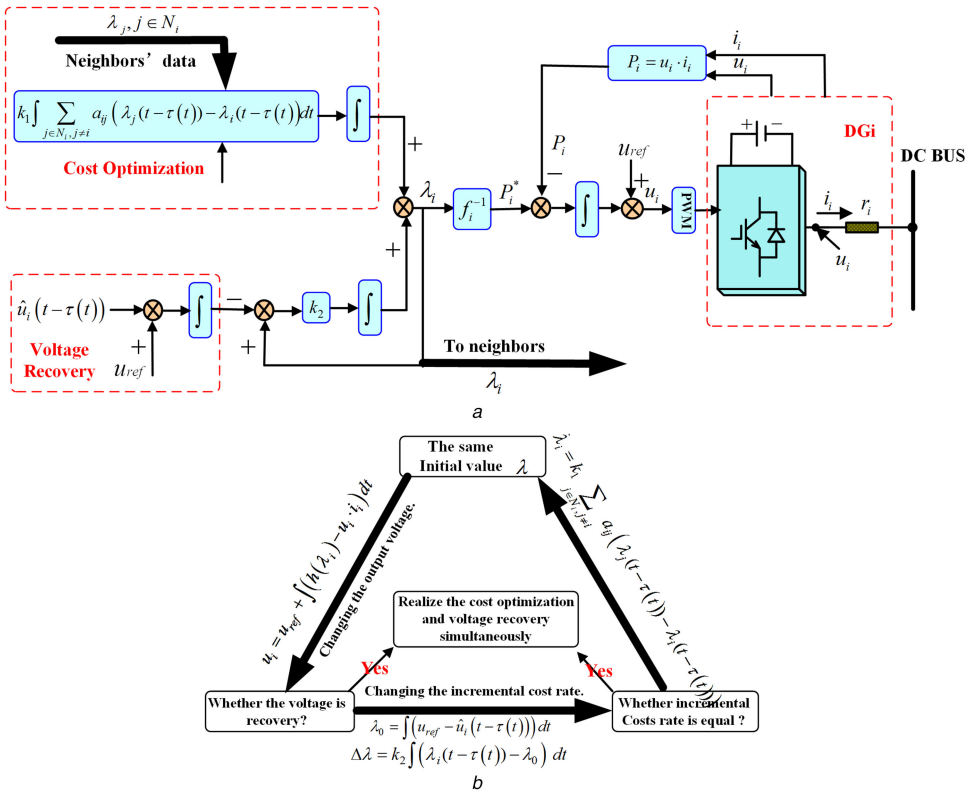

Fig. 2 *Schematic diagram of the proposed method*
(a) Detailed configuration of the proposed control system, ***(b)*** Process of incremental cost rate and power output control

$$\begin{cases} u_i = u_{\text{ref}} + \int (h(\lambda_i) - u_i \cdot i_i)\,\mathrm{d}t \\ \dot{\lambda}_i = k_1 \sum\limits_{j \in N_i, j \neq i} a_{ij}\big(\lambda_j(t-\tau(t)) - \lambda_i(t-\tau(t))\big) - k_2(\lambda_i(t-\tau(t)) - \lambda_0) \\ \lambda_0 = \int (u_{\text{ref}} - \hat{u}_i(t-\tau(t)))\,\mathrm{d}t \end{cases} \tag{10a–c}$$

where u_{ref} is the rated voltage, u_i is the actual output voltage of the ith DG, a_{ij} is the communication weight, and λ_i is a variable. $h(\lambda_i)$, which is the inverse function of $f_i(P_i)$, indirectly reflects the cost function. $\tau(t)$ is the communication delay, N_i denotes the set of all the neighbours of the ith DG, k_1 and k_2 express the positive gain coefficients, and $\hat{u}_i$ represents the local estimates of averaging voltages, which is used to restore the voltage of all DGs, and is introduced in detail below. A schematic diagram of the proposed method is shown in Fig. 2*a*.

$a_{ij} = 1$, if there is a communication link allowing information flow from the ith to the jth DG; otherwise, $a_{ij} = 0$. $\boldsymbol{A} = [k_1 a_{ij}]$ is a matrix, the main diagonal elements of which are all equal to 0 and $\text{rank}(\boldsymbol{A}) = n$, so that we can guarantee $\lambda_1 = \lambda_2 = \cdots = \lambda_n$. However, when a DG contacts only one other DG, some DGs are susceptible to losing connectivity in the case of a single-link failure, and the robustness of the system is weak. The corresponding DG can easily lose its connectivity, which hinders the functionality of the control mechanism.

As shown in Fig. 2*a*, the proposed method contains a cost optimisation module and a voltage regulation module. For the cost optimisation module, each DG obtains its neighbours' estimated value λ_j and local incremental cost rate estimated value λ_i, which includes the communication delay, $\tau(t)$. The distributed controller minimises the total generation cost by driving the incremental costs of all DGs to reach consensus.

The voltage regulation module can regulate the global average voltage of each DG. For each DG, a distributed algorithm is used to acquire the global average voltage, which considers the existing communication delay $\tau(t)$. The cooperative distributed approach for the global averaging voltage is described in Section 3.2.

As shown in Fig. 2*b*, each DG has the same initial incremental cost rate, and the DGs can achieve the output power under an equal incremental cost rate. However, the output voltage does not necessarily reach the rated voltage, and then, each DG regulates the output voltage to the global averaging voltage, and finally achieves the equal incremental rate under the premise of satisfying voltage recovery. Thus, both economic operation and the voltage quality of DC microgrids are guaranteed eventually.

3.2 Global average output voltage

A centralised hierarchical multilevel controller is the controller most frequently used in microgrids. However, it requires a heavy communication network and presents a single point of failure. In [19, 20], a distributed control strategy for global average voltage restoration between DGs in DC microgrids was presented.

The average state estimator implements the following distributed average consensus protocol [19]:

$$\hat{u}_i(t) = u_i(t) + \int_0^t \sum_{j \in N_i} a_{ij}\big(\hat{u}_j(\tau) - \hat{u}_i(\tau)\big)\,\mathrm{d}\tau \tag{11}$$

where $\hat{u}_i$ is the local estimate of the average voltage, u_i is the output voltage, and N_i expresses that the ith DG receives average state estimates from its neighbours.

According to (11), when a microgrid containing n DGs operates in steady state, the local voltage estimates of each DG are the same, which are equal to the global average output voltage, namely

$$\hat{u}_1 = \hat{u}_2 = \cdots = \hat{u}_n = \frac{u_1 + u_2 + \cdots + u_n}{n} \tag{12}$$

4 DC microgrids stability analysis

4.1 Steady-state analysis

A definite system including DGs, a resistive load, and line resistances, can be regarded as an n-port network, where all DGs and loads are nodes. When the system is in steady state, according to Kirchhoff's voltage and current theorem [30]

$$\begin{bmatrix} \boldsymbol{i} \\ \boldsymbol{i}_{\text{load}} \end{bmatrix} = \begin{bmatrix} \boldsymbol{L}_{ss} & \boldsymbol{L}_{sl} \\ \boldsymbol{L}_{ls} & \boldsymbol{L}_{ll} \end{bmatrix} \begin{bmatrix} \boldsymbol{u} \\ \boldsymbol{u}_{\text{load}} \end{bmatrix} \tag{13}$$

where $\boldsymbol{u} = [u_1\ u_2\ \cdots\ u_n]^{\mathrm{T}}$, $\boldsymbol{i} = [i_1\ i_2\ \cdots i_n]^{\mathrm{T}}$, $\boldsymbol{u}_{\text{load}} = [u_{\text{load}1}\ u_{\text{load}2}\ \cdots\ u_{\text{load}n}]^{\mathrm{T}}$, $\boldsymbol{i}_{\text{load}} = [i_{\text{load}1}\ i_{\text{load}2}\ \cdots\ i_{\text{load}n}]^{\mathrm{T}}$, $\boldsymbol{L}_{ss} \in \boldsymbol{R}^{n\times n}$, $\boldsymbol{L}_{sl} \in \boldsymbol{R}^{n\times m}$, $\boldsymbol{L}_{ls} \in \boldsymbol{R}^{m\times n}$, and $\boldsymbol{L}_{ll} \in \boldsymbol{R}^{m\times m}$ are constant matrices, which are determined by the line resistance and load of the system. The load node is

$$i_{\text{load}i} = R_i \cdot u_{\text{load}i} \tag{14}$$

where $\boldsymbol{R} = \text{diag}\{R_i\}$. According to (13) and (14), we have

$$\boldsymbol{i} = \boldsymbol{Y}\boldsymbol{u} \tag{15}$$

where $\boldsymbol{Y} = \boldsymbol{L}_{ss} + \boldsymbol{L}_{sl}\boldsymbol{R}(\boldsymbol{I} - \boldsymbol{L}_{ll}\boldsymbol{R})^{-1}\boldsymbol{L}_{ls} = \boldsymbol{L}_{ss} - \boldsymbol{L}_{sl}\left(\boldsymbol{L}_{ll} - \boldsymbol{R}^{-1}\right)^{-1}\boldsymbol{L}_{ls}$, which is an admittance matrix, and $\boldsymbol{I} = \text{diag}\{1\}$. According to the cost optimisation module, the distributed controller minimises the total generation cost by driving the incremental costs rate of all DGs to reach consensus. When the system operates in steady state, all the incremental costs rates, λ_i, are equal, namely

$$\lambda_1 = \lambda_2 = \cdots = \lambda_n \tag{16}$$

Based on the voltage restoration module, the global average output voltage can be restored. When the system is in steady state

$$\frac{u_1 + u_2 + \cdots + u_n}{n} = u_{\text{ref}} \tag{17}$$

$$h(\lambda_i) = u_i \cdot i_i \tag{18}$$

By using (15)–(18), the incremental costs rate $\bar{\lambda}_i (i = 1, 2, \ldots, n)$, output voltage $\bar{u}_i (i = 1, 2, \ldots, n)$, and current $\bar{i}_i (i = 1, 2, \ldots, n)$ of each DG in steady state can be solved.

4.2 Stability analysis

In this study, two classes of uncertainties, communication delay $\tau(t)$ and load change, were investigated.

The dynamics function of the output voltage u_i and cost increment rate λ_i is represented by (10). The derivation on both sides of (10) is taken, and we obtain (see (19)) where $d_i = \sum_{j\in N_i} a_{ij}$ and the time delay $\tau(t)$ is a time-varying differentiable function that satisfies

$$0 \le \tau(t) \le c \text{ and } |\dot{\tau}(t)| < \mu \tag{20}$$

where $c > 0$ and μ are constants.

When the system is in steady state, the local estimate of average voltage $\hat{u}_i$ and the actual global average voltage are equal, and meet the condition represented by (12).

Let $\boldsymbol{K}_1 = \text{diag}\{k_1 d_1\}, \boldsymbol{K}_2 = \text{diag}\{k_2\}, \boldsymbol{L} = \boldsymbol{K}_1 + \boldsymbol{K}_2 - \boldsymbol{A}$. When the system operates in the equilibrium point, the linearisation function of the output voltage and incremental cost rate can be described as

$$\begin{cases} \Delta\dot{\boldsymbol{u}} = \dfrac{\partial \boldsymbol{h}}{\partial \boldsymbol{\lambda}}\Delta\boldsymbol{\lambda} - \left(\bar{\boldsymbol{u}} \cdot \boldsymbol{Y} + \bar{\boldsymbol{i}}\right)\Delta\boldsymbol{u} \\ \Delta\dot{\boldsymbol{\lambda}} = -\boldsymbol{L}\Delta\boldsymbol{\lambda}(t - \tau(t)) + \boldsymbol{K}_2\Delta\boldsymbol{\lambda}_0 \\ \Delta\dot{\boldsymbol{\lambda}}_0 = \boldsymbol{C}\Delta\boldsymbol{u}(t - \tau(t)) \end{cases} \tag{21}$$

where $(\partial \boldsymbol{h}/\partial\boldsymbol{\lambda}) = \text{diag}(\partial h/\partial\lambda_i) = \boldsymbol{H}$, which is a diagonal matrix, $\Delta\dot{\boldsymbol{\lambda}} = [\Delta\lambda_1, \Delta\lambda_2, \ldots, \Delta\lambda_n]^{\mathrm{T}}$, $\Delta\boldsymbol{u} = [\Delta u_1, \Delta u_2, \ldots, \Delta u_i]^{\mathrm{T}}$, $\Delta\boldsymbol{i} = [\Delta i_1, \Delta i_2, \ldots, \Delta i_i]^{\mathrm{T}}$, $\bar{\boldsymbol{u}} = \text{diag}[\bar{u}_1, \bar{u}_2, \ldots, \bar{u}_n]$, and $\bar{\boldsymbol{i}} = \text{diag}\left[\bar{i}_1, \bar{i}_2, \ldots, \bar{i}_n\right]$. $\boldsymbol{C} \in \boldsymbol{R}^{n\times n}$ is a matrix, all the elements of which are equal to $1/n$.

When the load changes, the admittance matrix $\boldsymbol{Y}$ follows the change. Thus, $\boldsymbol{Y}$ is not a fixed matrix. When a change in the load is considered (see (22)) where $\Delta\boldsymbol{R} \ll \boldsymbol{R}$, because the change in a single load is small. Let $\boldsymbol{W} + \Delta\boldsymbol{W} = \bar{\boldsymbol{i}} + \bar{\boldsymbol{u}} \cdot \boldsymbol{Y}$ and $\Delta\boldsymbol{W}$ express the load change uncertainty

$$\begin{cases} \boldsymbol{W}_{\max} = \bar{\boldsymbol{i}} + \bar{\boldsymbol{u}}\left(\boldsymbol{L}_{ss} + \boldsymbol{L}_{sl}\left(\boldsymbol{L}_{ll} - \boldsymbol{R}^{-1}\right)^{-1}\boldsymbol{L}_{ls}\right) \\ \Delta\boldsymbol{W}_{\max} = -\bar{\boldsymbol{u}}\boldsymbol{L}_{sl}(\boldsymbol{R}\boldsymbol{L}_{ll} - \boldsymbol{I})^{-1}\Delta\boldsymbol{R}(\boldsymbol{L}_{ll}\boldsymbol{R} - \boldsymbol{I})^{-1}\boldsymbol{L}_{ls} \end{cases} \tag{23}$$

where $\Delta\boldsymbol{R}_{\max} = \boldsymbol{R}_{\max} - \boldsymbol{R}_{\min}$. When the system operates in steady state, let $\boldsymbol{x}_1 = \Delta\boldsymbol{u}, \boldsymbol{x}_2 = \Delta\boldsymbol{\lambda}, \boldsymbol{x}_3 = \Delta\boldsymbol{\lambda}_0$; then, (21) can be described as

$$\begin{cases} \dot{\boldsymbol{x}}_1 = -(\boldsymbol{W} + \Delta\boldsymbol{W})\boldsymbol{x}_1(t) + \mathbf{H}\boldsymbol{x}_2(t) \\ \dot{\boldsymbol{x}}_2 = -\boldsymbol{L}\boldsymbol{x}_2(t - \tau(t)) + \boldsymbol{K}_2\boldsymbol{x}_3(t) \\ \dot{\boldsymbol{x}}_3 = \boldsymbol{C}\boldsymbol{x}_1(t - \tau(t)) \end{cases} \tag{24}$$

Accordingly, we can obtain

$$\dot{\boldsymbol{x}} = (\boldsymbol{A}_b + \boldsymbol{\Delta}\boldsymbol{A}_b(t))\boldsymbol{x}(t) + \boldsymbol{A}_d\boldsymbol{x}(t - \tau(t)) \tag{25}$$

$$\begin{cases} \dot{u}_i = h(\lambda_i) - u_i \cdot i_i, \quad i \in 1, 2, \ldots, n \\ \dot{\lambda}_i = k_1 \cdot \sum\limits_{j\in N_i, j\neq i} a_{ij}\lambda_j(t - \tau(t) - k_1 d_i\lambda_i(t - \tau(t)) - k_2(\lambda_i(t - \tau(t) - \lambda_0) \\ \dot{\lambda}_0 = u_{ref} - \hat{u}_i(t - \tau(t)) \end{cases} \tag{19}$$

$$\begin{aligned} \boldsymbol{Y}(\boldsymbol{R} + \Delta\boldsymbol{R}) &= \boldsymbol{L}_{ss} - \boldsymbol{L}_{sl}\left(\boldsymbol{L}_{ll} - (\boldsymbol{R} + \Delta\boldsymbol{R})^{-1}\right)^{-1}\boldsymbol{L}_{ls} \\ &= \boldsymbol{L}_{ss} - \boldsymbol{L}_{sl}\left(\boldsymbol{L}_{ll} - \left(\boldsymbol{I} + \boldsymbol{R}^{-1}\Delta\boldsymbol{R}\right)^{-1}\boldsymbol{R}^{-1}\right)^{-1}\boldsymbol{L}_{ls} \\ &\simeq \boldsymbol{L}_{ss} - \boldsymbol{L}_{sl}\left(\boldsymbol{L}_{ll} - \boldsymbol{R}^{-1} - \boldsymbol{R}^{-1}\Delta\boldsymbol{R}\boldsymbol{R}^{-1}\right)^{-1}\boldsymbol{L}_{ls} \\ &= \boldsymbol{L}_{ss} + \boldsymbol{L}_{sl}\left(\boldsymbol{I} - \left(\boldsymbol{L}_{ll} - \boldsymbol{R}^{-1}\right)^{-1}\boldsymbol{R}^{-1}\Delta\boldsymbol{R}\boldsymbol{R}^{-1}\right)^{-1}\left(\boldsymbol{L}_{ll} - \boldsymbol{R}^{-1}\right)^{-1}\boldsymbol{L}_{ls} \\ &\simeq \boldsymbol{L}_{ss} + \boldsymbol{L}_{sl}\left(\boldsymbol{I} - \left(\boldsymbol{L}_{ll} - \boldsymbol{R}^{-1}\right)^{-1}\boldsymbol{R}^{-1}\Delta\boldsymbol{R}\boldsymbol{R}^{-1}\right)\left(\boldsymbol{L}_{ll} - \boldsymbol{R}^{-1}\right)^{-1}\boldsymbol{L}_{ls} \\ &= \boldsymbol{L}_{ss} + \boldsymbol{L}_{sl}\left(\boldsymbol{L}_{ll} - \boldsymbol{R}^{-1}\right)^{-1}\boldsymbol{L}_{ls} - \boldsymbol{L}_{sl}\left(\boldsymbol{L}_{ll} - \boldsymbol{R}^{-1}\right)^{-1}\boldsymbol{R}^{-1}\Delta\boldsymbol{R}\boldsymbol{R}^{-1}\left(\boldsymbol{L}_{ll} - \boldsymbol{R}^{-1}\right)^{-1}\boldsymbol{L}_{ls} \\ &= \boldsymbol{L}_{ss} + \boldsymbol{L}_{sl}\left(\boldsymbol{L}_{ll} - \boldsymbol{R}^{-1}\right)^{-1}\boldsymbol{L}_{ls} - \boldsymbol{L}_{sl}(\boldsymbol{R}\boldsymbol{L}_{ll} - \boldsymbol{I})^{-1}\Delta\boldsymbol{R}(\boldsymbol{L}_{ll}\boldsymbol{R} - \boldsymbol{I})^{-1}\boldsymbol{L}_{ls} \end{aligned} \tag{22}$$

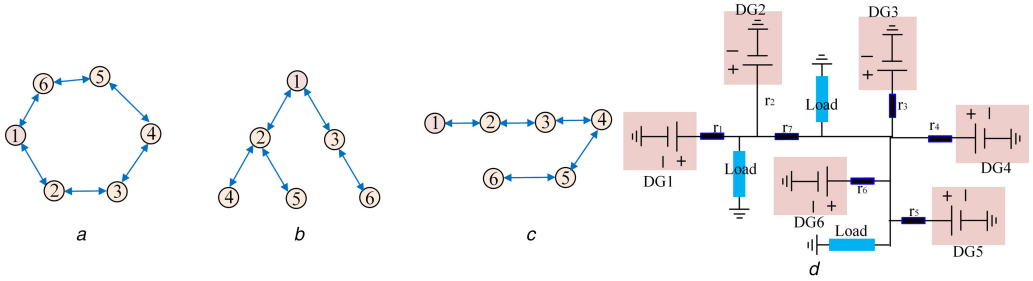

Fig. 3 *Communication topology and physical connection of the DC microgrid*
(a) Ring-shaped topology, ***(b)*** Tree-shaped topology, ***(c)*** Line-shaped topology, ***(d)*** Physical connection

Table 1 Simulink parameters of the DC microgrid

Item	Symbol
inductance of six converters	$L_1 = L_2 = L_3 = 0.65$ mH, $L_4 = L_5 = L_6 = 0.75$ mH
capacitance of six converters	$C_1 = C_2 = C_3 = 94$ μF, $C_4 = C_5 = C_6 = 150$ μF
line resistance	$r_1 = r_4 = 0.5\ \Omega$, $r_2 = r_6 = 0.4\ \Omega$, $r_3 = r_5 = r_7 = 0.3\ \Omega$
input voltage of converter	200 V

where $\dot{\boldsymbol{x}} = [\dot{\boldsymbol{x}}_1 \quad \dot{\boldsymbol{x}}_2 \quad \dot{\boldsymbol{x}}_3]^{\mathrm{T}}$

$$\boldsymbol{A}_b = \begin{bmatrix} -\boldsymbol{W} & \boldsymbol{H} & \boldsymbol{O} \\ \boldsymbol{O} & \boldsymbol{O} & \boldsymbol{K}_2 \\ \boldsymbol{O} & \boldsymbol{O} & \boldsymbol{O} \end{bmatrix}, \quad \Delta\boldsymbol{A}_b = \begin{bmatrix} -\Delta\boldsymbol{W} & \boldsymbol{O} & \boldsymbol{O} \\ \boldsymbol{O} & \boldsymbol{O} & \boldsymbol{O} \\ \boldsymbol{O} & \boldsymbol{O} & \boldsymbol{O} \end{bmatrix}, \quad \boldsymbol{A}_d = \begin{bmatrix} \boldsymbol{O} & \boldsymbol{O} & \boldsymbol{O} \\ \boldsymbol{O} & -\boldsymbol{L} & \boldsymbol{O} \\ \boldsymbol{C} & \boldsymbol{O} & \boldsymbol{O} \end{bmatrix}.$$

The uncertainties are assumed to be of the form

$$[\Delta\boldsymbol{A}_b(t)] = \boldsymbol{D}\boldsymbol{F}(t)\boldsymbol{E}_a \tag{26}$$

where $\boldsymbol{D} = |\Delta\boldsymbol{W}_{\max}|\boldsymbol{I}$. $\boldsymbol{E}_a$ is a constant matrix with appropriate dimensions and $\boldsymbol{F}^{\mathrm{T}}(t)$ is unknown and real-valued, and satisfies $\boldsymbol{F}^{\mathrm{T}}(t)\boldsymbol{F}(t) \le \boldsymbol{I}$.

In (25), the two classes of uncertainties, time-varying delay $\tau(t)$ and load change, are considered. The robust stability conditions for this system are discussed in the following.

Given delay $c > 0$ and μ, the system represented by (25) is robustly stable (for details of the Lyapunov function, see [31]) if there exist matrices $\boldsymbol{P} = \boldsymbol{P}^{\mathrm{T}} > 0$, $\boldsymbol{Q} = \boldsymbol{Q}^{\mathrm{T}} \ge 0$, $\boldsymbol{R}_1 = \boldsymbol{R}_1^{\mathrm{T}} \ge 0$, $\boldsymbol{Z}_i = \boldsymbol{Z}_i^{\mathrm{T}} > \boldsymbol{0}, i = 1, 2$, $\boldsymbol{N} = [\boldsymbol{N}_1 \quad \boldsymbol{N}_2 \quad \boldsymbol{N}_3]^{\mathrm{T}}$, $\boldsymbol{S} = [\boldsymbol{S}_1 \quad \boldsymbol{S}_2 \quad \boldsymbol{S}_3]^{\mathrm{T}}$, $\boldsymbol{M} = [\boldsymbol{M}_1 \quad \boldsymbol{M}_2 \quad \boldsymbol{M}_3]^{\mathrm{T}}$, where $\boldsymbol{N}$, $\boldsymbol{S}$, and $\boldsymbol{M}$ are freedom matrices, and a scalar $\lambda > 0$, such that the following LMI holds:

$$\begin{bmatrix} \hat{\boldsymbol{\Phi}} & c\boldsymbol{N} & c\boldsymbol{S} & c\boldsymbol{M} & c\boldsymbol{A}_{c1}^{\mathrm{T}}\hat{\boldsymbol{Z}} & \hat{\boldsymbol{P}}\boldsymbol{D} \\ * & -c\boldsymbol{Z}_1 & \boldsymbol{O} & \boldsymbol{O} & \boldsymbol{O} & \boldsymbol{O} \\ * & * & -c\boldsymbol{Z}_1 & \boldsymbol{O} & \boldsymbol{O} & \boldsymbol{O} \\ * & * & * & -c\boldsymbol{Z}_2 & \boldsymbol{O} & \boldsymbol{O} \\ * & * & * & * & -c\hat{\boldsymbol{Z}} & -c\boldsymbol{Z}_1\boldsymbol{D} \\ * & * & * & * & * & -\lambda\boldsymbol{I} \end{bmatrix} < 0 \tag{27}$$

where (see equation below) and * denotes the symmetric terms in a symmetric matrix.

There exist exact matrices $\boldsymbol{A}_b, \boldsymbol{A}_d, \boldsymbol{D}$, and $\boldsymbol{E}_a$ for a definite system, and then the delay upper bound c can be obtained based on (27).

5 Simulation results

The performance validation of the proposed scheme was conducted for the microgrid configuration shown in Fig. 3*d*. To simplify the model, the simulation was conducted using a system having six DGs. The simulation parameters are shown in Table 1. The microgrid voltage was set as 200 V ± 10%. At $t = 0$ s, the load power was 1 kW. At $t = 3$ and 6 s, the load power changed from 1 to 2 kW and to 4 kW, respectively. We could observe the change in the output power of each DG accordingly when the load changed. The selected communication topologies are depicted in Fig. 3 (the communication topology of all the simulations is shown in Fig. 3*a*, except Case III).

According to (1) and (2), the common cost function of DGs can be expressed as

$$C_i(P_i) = a + bP_i + cP_i^2 + d\exp(eP_i) \tag{28}$$

DG1 and DG2 are DC diesel generators and DG3 and DG4 are electric generators driven by a micro turbine. DG5 and DG6 are assumed to be dispatchable sources, such as a solar or wind generator. The parameters for the cost function of DGs are listed in Table 2.

The robust stability of a microgrid system (24) with six DGs was analysed. When $P_{\mathrm{load}} = 1$ kW, according to LMI (27) we can obtain the relationship between the integral gain and the upper bound of the delay. As shown in Fig. 4, with the increase in the gain k_1 or k_2, the conclusion can be drawn that the upper bound c of the system is gradually reduced. Fig. 4 shows a comparison of the upper bound of c of the system and a delay of 100 ms.

By using (5) and (9), we can obtain the theory relationship of the load power and optimal output power of each DG, as shown in Fig. 5*a*. The power values are also listed in the figure. The

$$\hat{\boldsymbol{\Phi}} = \boldsymbol{\Phi} + \begin{bmatrix} \lambda\mathbf{E}_a^{\mathrm{T}}\mathbf{E}_a & \mathbf{O} & \mathbf{O} \\ * & \mathbf{O} & \mathbf{O} \\ * & * & \mathbf{O} \end{bmatrix}, \quad \hat{\mathbf{P}} = \begin{bmatrix} \mathbf{P} \\ 0 \\ 0 \end{bmatrix}, \quad \hat{\mathbf{Z}} = \mathbf{Z}_1 + \mathbf{Z}_2, \quad \boldsymbol{\Phi} = \boldsymbol{\Phi}_1 + \boldsymbol{\Phi}_2 + \boldsymbol{\Phi}_2^{\mathrm{T}},$$

$$\boldsymbol{\Phi}_1 = \begin{bmatrix} \mathbf{P}\mathbf{A}_b + \mathbf{A}_b^{\mathrm{T}}\mathbf{P} + \mathbf{Q} + \mathbf{R}_1 & \mathbf{P}\mathbf{A}_d & \mathbf{O} \\ * & -(1-\mu)\mathbf{Q} & \mathbf{O} \\ * & * & -\mathbf{R}_1 \end{bmatrix}, \quad \boldsymbol{\Phi}_2 = [\mathbf{N} + \mathbf{M} \quad -\mathbf{N} + \mathbf{S} \quad -\mathbf{M} - \mathbf{S}], \quad \mathbf{A}_{c1} = [\mathbf{A}_b \quad \mathbf{A}_d \quad \mathbf{O}]$$

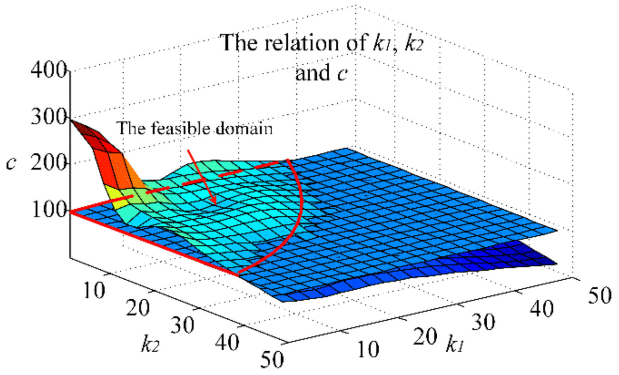

Fig. 4 *Relationship of c and k_1, k_2*

normalised generation cost curve according to (3) is shown in Fig. 5*b*.

For the proposed control method, each DG needs to exchange only the estimated value of the incremental cost rate with its neighbours. Fig. 5*c* shows the real-time incremental cost rate of the six DGs. In this figure, it can be seen that the output power of the system is always optimal because the incremental cost rate is always equal for all DGs. The cost incremental rate of each DG shown in Fig. 5*d* was achieved by using the control method proposed in [17]. As compared with that shown in Fig. 5*d*, the transient performance shown in Fig. 5*c* is good.

5.1 Case I: With and without communication delay

First, the DGs' controllers are designed according to the proposed control scheme without taking communication delay into consideration. Figs. 6*a* and *b* show the variations in the output voltage and power under three different conditions of loads when the proposed scheme was implemented. As shown in Fig. 6*a*, the output voltage of the six DGs is regulated, and close to the reference voltage. Fig. 6*b* shows that the DGs in general generate power in accordance with the relationship between the load power and the DG optimal output power shown in Fig. 5*a*. The deviation between the output power shown in Fig. 6*b* and that shown in Fig. 5*a* is caused by the line loss.

Taking the communication delay into consideration, the feasibility of the proposed control scheme was analysed. As shown in Figs. 6*c* and *d*, the output voltage and the active power oscillate at the beginning of the implementation of the proposed method, eventually stabilising after a short transient time. This shows that the proposed method can be used even under communication delay conditions.

5.2 Case II: Analysis of delay τ and gain

After the communication delay had been considered, the performance of DGs was analysed in the case where the delay, τ, changes. As the value of τ increases, the oscillation time of the system increases. As compared with those shown in Figs. 7*a* and *b*, the convergence speeds shown in Figs. 7*c* and *d* are slower. This indicates that a small time delay would lead to a better control performance. When the delay is within the maximum allowable delay bound, the output voltage and the active power are stabilised eventually after a transient time. However, when the value of τ exceeds the maximum allowable delay bound c according to LMI, the proposed control method cannot be implemented. As shown in Figs. 7*c* and *d*, when the load resistance is 1 kW, τ reaches the delay upper bound c, and the system becomes unstable. When the load resistance is increased, the delay upper bound c is increased, which means that the system can operate normally.

As an important variable, the influence of gain k_2 is analysed. A comparison of Figs. 8*b* and *d* reveals that a smaller k_2 can enhance the system stability and improve the transient behaviour.

Table 2 Cost function of the distributed generators

Item	a (10^{-2})	b (10^{-1})	c (10^{-1})	d (10^{-1})	e (10^{-3})	P^{min}, kW	P^{max}, kW
DG1	64	1.2	8.6	2	1	0	1
DG2	74	1	10.6	3	1	0	1
DG3	60	1.6	5	1	1	0	1
DG4	105.9	1.9	7.2	1	1	0	1
DG5	0.36	1.97	0.8	0	0	0	2
DG6	0.08	0.985	1	0	0	0	2

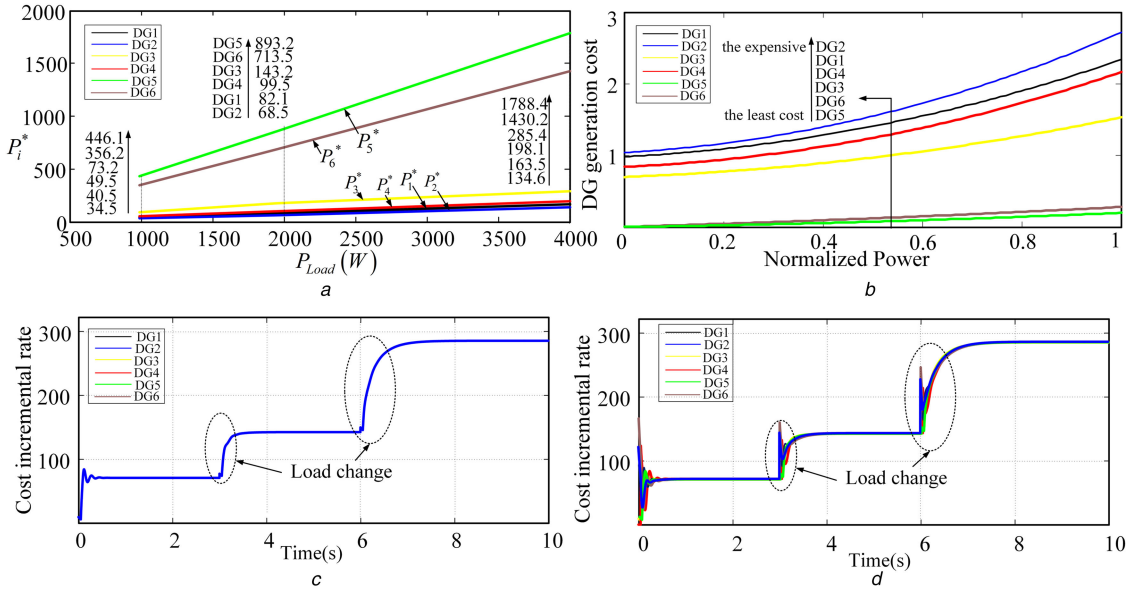

Fig. 5 *Simulation results*

(a) Relationship between load power and distributed generator optimal output power, ***(b)*** DGs' generation cost curves, ***(c)*** Cost incremental rate of each DG for the proposed control, ***(d)*** Cost incremental rate of each DG for the method in [17]

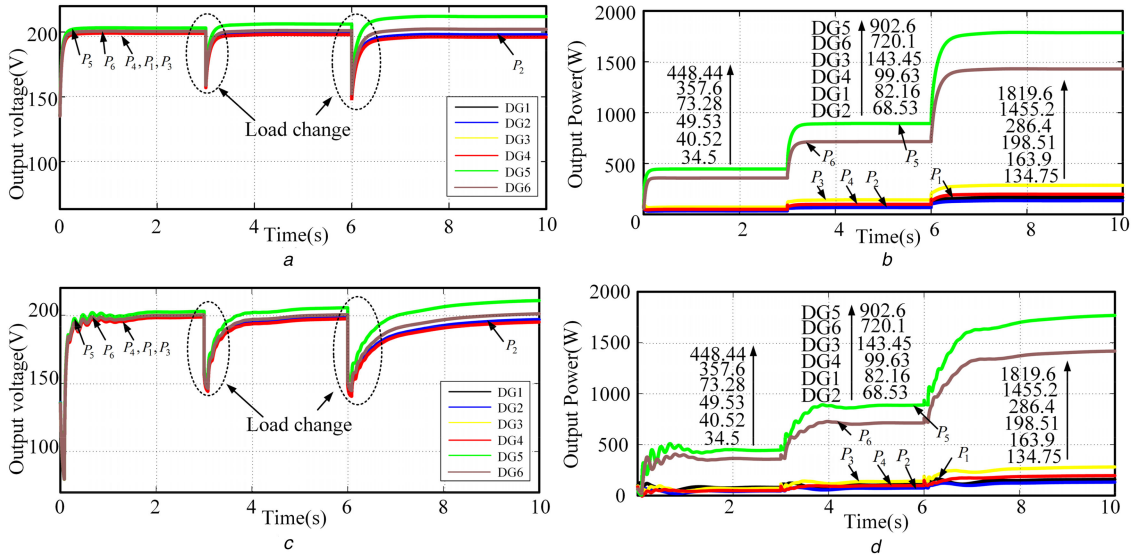

Fig. 6 *Active power and output voltage of distributed generators with and without communication delay*

(a) DGs' output voltage with $k_1 = 20, k_2 = 30, \tau = 0$ s, ***(b)*** DGs' output power with $k_1 = 20, k_2 = 30, \tau = 0$ s, ***(c)*** DGs' output voltage with $k_1 = 20, k_2 = 30, \tau = 0.08$ s, ***(d)*** DGs' output power with $k_1 = 20, k_2 = 30, \tau = 0.08$ s

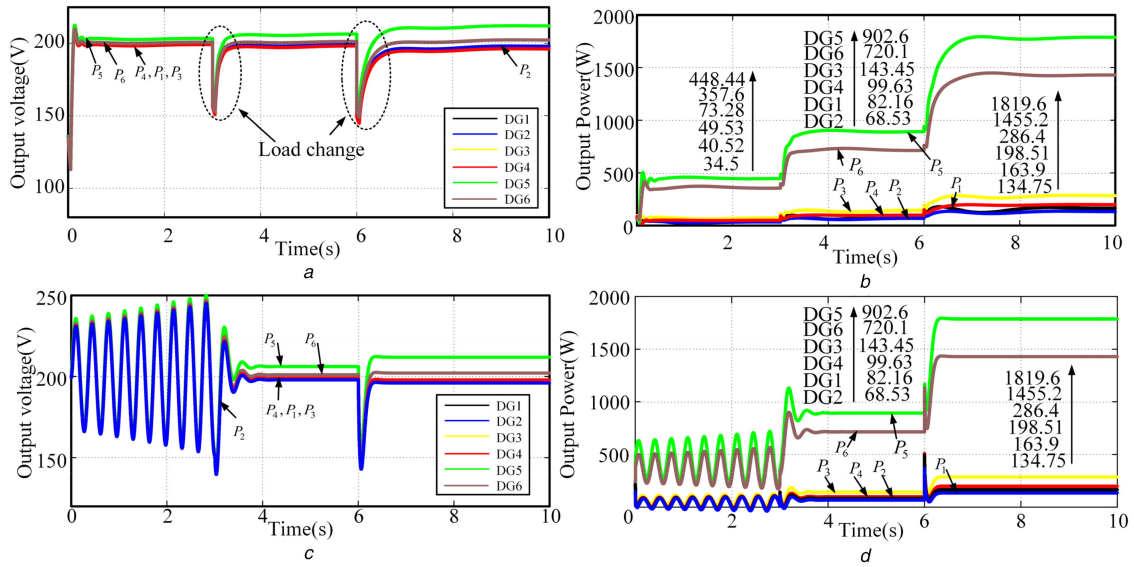

Fig. 7 *Active power and output voltage of distributed generators with different load resistance values*

(a) DGs' output voltage with $k_1 = 20, k_2 = 10, \tau = 0.05$ s, ***(b)*** DGs' output power with $k_1 = 20, k_2 = 10, \tau = 0.05$ s, ***(c)*** DGs' output voltage with $k_1 = 20, k_2 = 10, \tau = 0.291$ s, ***(d)*** DGs' output power with $k_1 = 20, k_2 = 10, \tau = 0.291$ s

5.3 Case III: Analysis of changes in communication topology

We examined the control performance of the proposed scheme under ring-, tree-, and line-shaped communication networks, as shown in Fig. 3, in the presence of time delay. The load resistance was maintained at 1 kW. As compared with the convergence speeds of the topologies shown in Figs. 9 and 10, it can be concluded that a line-shaped is faster than a tree- or ring-shaped communication network, and the tree-shaped network is the slowest. This is because the different systems with different topology structures have different connectivity, and this may lead to a different spectral radius, which determines the convergence speed. The access of the load also influences the convergence speeds with different topologies.

6 Experimental results

The proposed distributed control method was experimentally verified. A microgrid consisting of three DGs based on the buck inverter was analysed (DG1, DG3, and DG5 examined in the simulation). The parameters for the output filter were the same as those in the simulation. The microgrid voltage was set as 48 V ± 10%. $k_1 = 10, k_2 = 10, \lambda = 0.04$ s. The test was performed under three different load conditions, including three resistors of 136, 218, and 270 W. Three inverters were used for the three DGs. The permissible minimum output voltage was not <90% of the rated voltage. The inverters were controlled using a TMS320f28335 digital signal processor. The experimental setup is shown in Fig. 11*a*.

The waveforms of the output currents of the three DGs and the load voltages are shown in Fig. 11*b*. It can be seen in Fig. 11*b* that the voltage in the load node is well-regulated. In the experiment, the current measured was that through the inductor. According to the schematic of the buck circuit, since the current of the capacitor can be ignored, the current through the inductor is approximately equal to the current through the line resistor. In the experimental data analysis process, the inductor current was expressed as the DG's output current. Fig. 12*b* shows the waveforms of the three DGs' output power using the experimental data. As compared with Fig. 12*a*, the experimental results are found to match in general with the theoretical optimal value based on (8). The deviation between the output power shown in Figs. 12*a* and *b* is because the line loss needs to be considered in the actual output power.

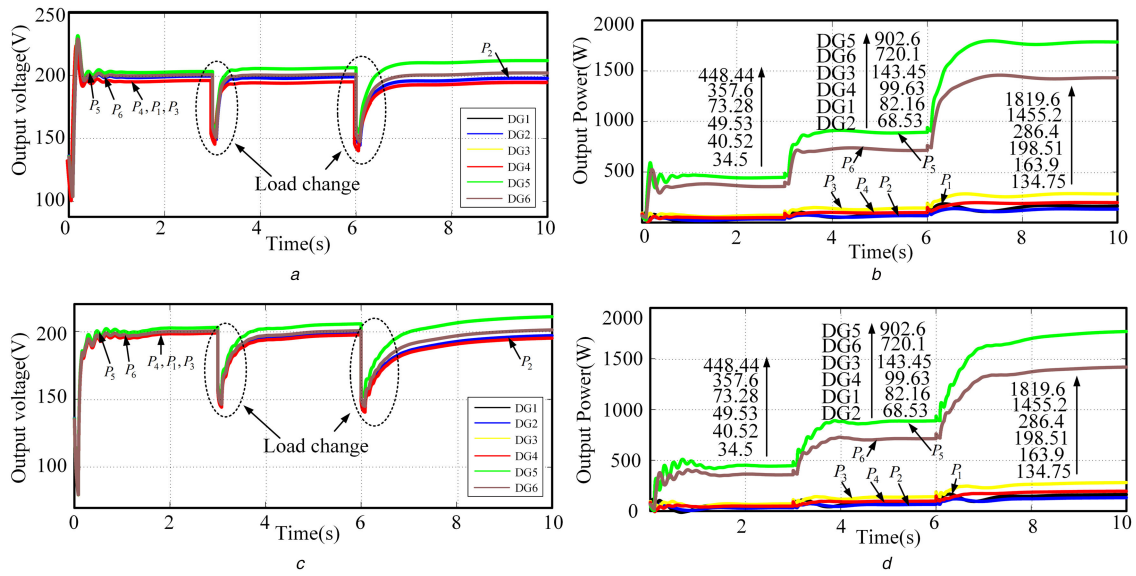

Fig. 8 *Active power and output voltage of distributed generators with different load resistance value*

(a) DGs' output voltage with $k_1 = 20, k_2 = 10, \tau = 0.08$ s, ***(b)*** DGs' output power with $k_1 = 20, k_2 = 10, \tau = 0.08$ s, ***(c)*** DGs' output voltage with $k_1 = 20, k_2 = 30, \tau = 0.08$ s, ***(d)*** DGs' output power with $k_1 = 20, k_2 = 30, \tau = 0.08$ s

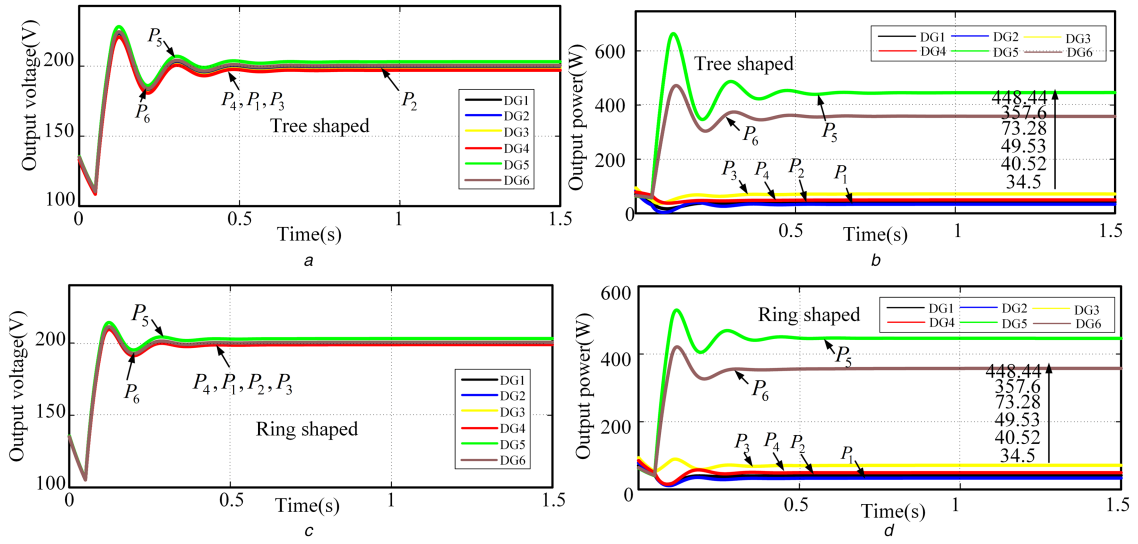

Fig. 9 *Active power and output voltage of distributed generators with different communication topologies when* $k_1 = 20, k_2 = 10, \tau = 0.05$ s

(a) DGs' output voltage with tree-shaped communication network, ***(b)*** DGs' output power with tree-shaped communication network, ***(c)*** DGs' output voltage with ring-shaped communication network, ***(d)*** DGs' output power with ring-shaped communication network

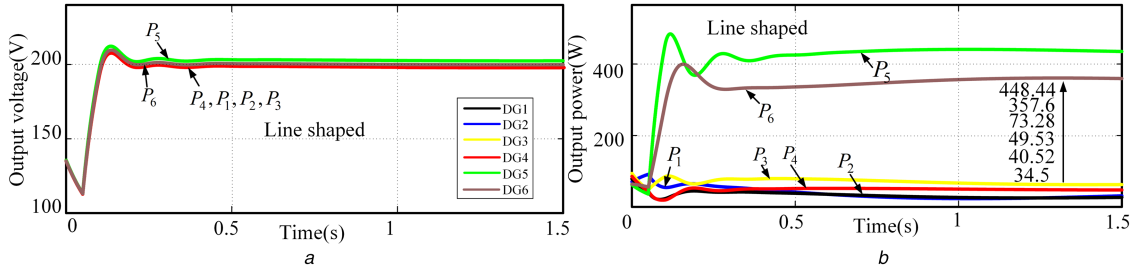

Fig. 10 *Active power and output voltage of distributed generators with different communication topologies when* $k_1 = 20, k_2 = 10, \tau = 0.05$ s

(a) DGs' output voltage with line-shaped communication network, ***(b)*** DGs' output power with line-shaped communication network

7 Conclusion

In this paper, a distributed optimisation control method based on a continuous-time DC microgrids system with communication delays was addressed. Even when the loads change and time-varying communication delays are present within the allowed delay upper bounds, the DC microgrid system based on the proposed control strategy can operate in cost optimal operation mode and it exhibits satisfactory transient performances. The criticalities of the robust stability of the system were obtained by LMI. The effectiveness of the proposed scheme was verified through simulations and experimentally.

8 Acknowledgments

This work was supported by the National Natural Science Foundation of China under Grant 61573384, the National High-tech R&D Program of China (863 Program) under Grant

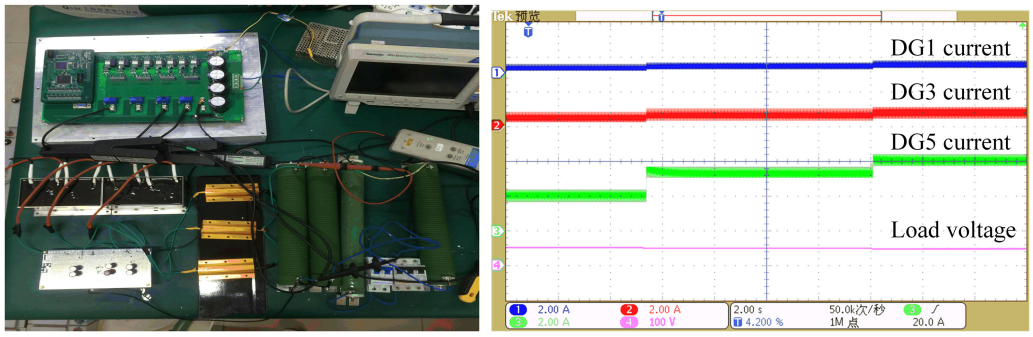

a *b*

Fig. 11 *Waveforms of the output currents of the three DGs and the load voltages*
(a) Experimental setup, ***(b)*** Output current and load voltage waveforms

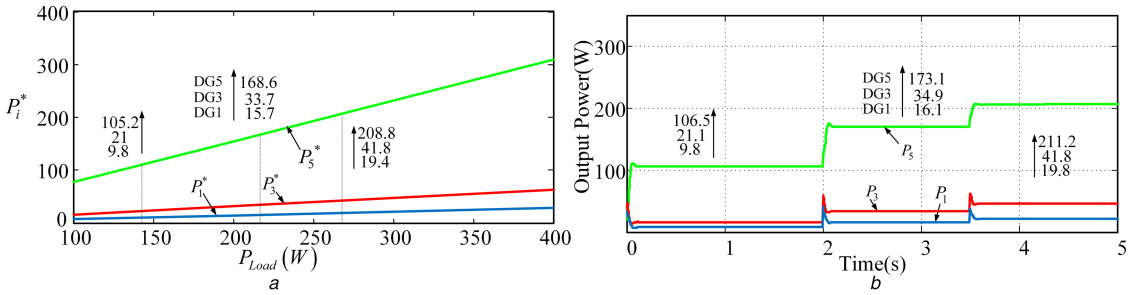

Fig. 12 *The theoretical values and the experimental values of the three DGs output power*
(a) Relationship between load power and distributed generator optimal output power, ***(b)*** Output power waveforms with the experimental data

2015AA050604, Central South University innovation-driven project and Natural Science Foundation of Hunan Province of China under Grant 2016JJ1019.

9 References

[1] Baran, M., Mahajan, N.: 'DC distribution for industrial systems: opportunities and challenges', *IEEE Trans. Ind. Electron.*, 2003, **39**, (6), pp. 1596–1601
[2] Su, M., Liu, Z., Sun, Y.,, *et al.*: 'Stability analysis and stabilization methods of DC microgrid with multiple parallel-connected DC-DC converters loaded by CPLs', *IEEE Trans. Smart Grid*, 2016, **PP**, (99), pp. 1–1, DOI: 10.1109/TSG.2016.2546551
[3] Han, H., Hou, X., Yang, J.,, *et al.*: 'Review of power sharing control strategies for islanding operation of AC microgrids', *IEEE Trans. Smart Grid*, 2016, **7**, (1), pp. 200–215
[4] Olivares, D., Canizares, C., Kazerani, M.: 'A centralized optimal energy management system for microgrids'. Proc. IEEE Power Energy Society General Meeting, 2011
[5] Tan, K., Peng, X., So, P.,, *et al.*: 'Centralized control for parallel operation of distributed generation inverters in microgrids', *IEEE Trans. Smart Grid*, 2012, **3**, (4), pp. 1977–1987
[6] Ahn, C., Peng, H.: 'Decentralized voltage control to minimize distribution power loss of microgrid', *IEEE Trans. Smart Grid*, 2013, **4**, (3), pp. 1297–1304
[7] Nutkani, I., Loh, P., Wang, P.,, *et al.*: 'Dcentralized economical dispatch scheme with online power reserve for microgrid', *IEEE Trans. Smart Grid*, 2017, **8**, (1), pp. 139–148
[8] Huang, P., Liu, P., Xiao, W.,, *et al.*: 'A novel droop-based average voltage sharing control strategy for DC microgrids', *IEEE Trans. Smart Grid*, 2015, **6**, (3), pp. 1096–1106
[9] Sun, Y., Hou, X., Yang, J.,, *et al.*: 'New perspectives on droop control in AC microgrid', *IEEE Trans. Ind. Electron.*, 2017, **64**, (17), pp. 5741–5745
[10] Nutkani, I., Loh, P., Wang, P.,, *et al.*: 'Autonomous droop scheme with reduced generation cost', *IEEE Trans. Ind. Electron.*, 2014, **61**, (12), pp. 6803–6811
[11] Nutkani, I., Loh, P., Wang, P.,, *et al.*: 'Cost-based droop scheme for DC microgrid'. Energy Conversion Congress and Exposition, 2014
[12] Lee, C.: 'A new droop control method for the autonomous operation of distributed energy resource interface converters', *IEEE Trans. Power Electron.*, 2013, **28**, (4), pp. 1980–1993
[13] Lu, J., Zhang, Y., Long, J.,, *et al.*: 'A novel virtual impedance method for droop controlled parallel UPS inverters with wireless control'. ITEC Asia-Pacific, 2014
[14] Zhang, Z., Chow, M.: 'Convergence analysis of the incremental cost consensus algorithm under different communication network topologies in a smart grid', *IEEE Trans. Power Syst.*, 2012, **27**, (4), pp. 1761–1768
[15] Yang, S., Tan, S., Xu, J.: 'Consensus based approach for economic dispatch problem in a smart grid', *IEEE Trans. Power Syst.*, 2013, **28**, (4), pp. 4416–4426
[16] Zhang, W., Liu, W., Wang, X.,, *et al.*: 'Online optimal generation control based on constrained distributed gradient algorithm', *IEEE Trans. Power Syst.*, 2015, **30**, (1), pp. 35–45
[17] Moayedi, S., Davoudi, A.: 'Unifying distributed dynamic optimization and control of islanded DC microgrids', *IEEE Trans. Power Electron.*, 2017, **32**, (3), pp. 2329–2346
[18] Wang, Z., Wu, W., Zhang, B.: 'A distributed control method with minimum generation cost for DC microgrids', *IEEE Trans. Energy Convers.*, 2016, **31**, (4), pp. 1462–1470
[19] Nasirian, V., Davoudi, A., Lewis, F.: 'Distributed adaptive droop control for DC distribution system', *IEEE Trans. Energy Convers.*, 2014, **29**, (4), pp. 944–956
[20] Nasirian, V., Moayedi, S., Davoudi, A.,, *et al.*: 'Distributed cooperative control of DC microgrid', *IEEE Trans. Power Electron.*, 2015, **30**, (4), pp. 2288–2303
[21] Zhou, Y., Huang, Z., Liu, W.,, *et al.*: 'A distributed ESO based cooperative current-sharing strategy for parallel charging systems under disturbances'. Energy Conversion Congress and Exposition, 2016, pp. 1–7
[22] Wang, F., Liang, J., Huang, T.: 'Synchronisation of stochastic delayed multi-agent systems with uncertain communication links and directed topologies', *IET Control Theory Appl.*, 2016, **11**, (1), pp. 90–100
[23] Xiang, J., Li, Y., Wei, W.,, *et al.*: 'Synchronisation of linear continuous multi-agent systems with switching topology and communication delay', *IET Control Theory Appl.*, 2014, **8**, (14), pp. 1415–1420
[24] Sun, Y., Wang, L.: 'Consensus of multi-agent systems in directed networks with nonuniform time-varying delays', *IEEE Trans. Autom. Control*, 2009, **54**, (7), pp. 1607–1613
[25] Carli, R., Chiuso, A., Schenato, L.,, *et al.*: 'Optimal synchronization for networks of noisy double integrators', *IEEE Trans. Autom. Control*, 2011, **56**, (5), pp. 1146–1152
[26] Nedic, A., Ozdaglar, A., Parrilo, P.A.: 'Constrained consensus and optimization in multi-agent networks', *IEEE Trans. Autom. Control*, 2010, **55**, (4), pp. 922–938
[27] Chen, G., Zhao, Z.: 'Delay effects on consensus-based distributed economic dispatch algorithm in microgrid', *IEEE Trans. Power Syst.*, 2016, **PP**, (99), pp. 1–1, DOI: 10.1109/TPWRS.2017.2702179
[28] Chen, G., Wen, C., Mao, J.,, *et al.*: 'Distributed economic dispatch for smart grids with random wind power', *IEEE Trans. Smart Grid*, 2016, **7**, (3), pp. 1572–1583
[29] Hetzer, J., Yu, D., Bhattarai, K.: 'An economic dispatch modeling cooperating wind power', *IEEE Trans. Energy Convers.*, 2008, **23**, (2), pp. 603–611
[30] Sun, Y., Zhang, G., Xu, W.,, *et al.*: 'A harmonically coupled admittance matrix model for AC/DC converters', *IEEE Trans. Power Syst.*, 2007, **22**, (4), pp. 1574–1582
[31] He, Y., Wang, Q., Xie, L.,, *et al.*: 'Further improvement of free-weighting matrices technique for systems with time-varying delay', *IEEE Trans. Autom. Control*, 2007, **52**, (2), pp. 293–299